

ASNOM mapping of SiC epi-layer doping profile and of surface phonon polariton waveguiding

Dmitry Kazantsev^{*,†,‡}

LEB, University of Erlangen, Cauerstr. 6, D-91058, Germany

E-mail: kaza@itep.ru

Abstract

The apertureless SNOM mapping of the slightly-doped 4H-SiC epitaxial layer grown on a heavily-doped 4H-SiC substrate was performed with a cleaved edge geometry. ASNOM images taken at the light frequencies of a $C^{13}O_2^{16}$ laser show a clear contrast between the substrate and the epitaxial layer. The contrast vanishes at the laser frequency of 884cm^{-1} , and gets clearer at higher frequencies (923cm^{-1}). This can be explained by changes in the local polarizability of SiC caused by the carrier concentration, which are more pronounced at higher frequencies. Since the light frequency is tuned up further (935cm^{-1}), a transversal mode structure appears in the ASNOM map, indicating a waveguide-like confinement of a surface phonon polariton wave inside the strip of an epi-layer outcrop.

Introduction

Recently, several papers report a successful application of an Apertureless Scanning Near-field Optical Microscopy (ASNOM, s-SNOM)^{1,2} to the mapping of a solid state surface optical properties.³⁻⁶ This method demonstrates not only the ability to distinguish different materials by their ASNOM response,⁷⁻¹⁰ but is even sensitive to the fine variations in an ASNOM response caused by

a presence of the free carriers in the same media.^{5,11,12}

Experimental

In the present paper, we report an ASNOM mapping of a SiC epitaxial layer (doping $n_N = 9 \cdot 10^{14}\text{cm}^{-3}$, thickness $d = 9.9\mu\text{m}$) grown on a SiC substrate (doping $n_N = 7 \cdot 10^{18}\text{cm}^{-3}$). Both the substrate and the epitaxial layer are of 4H polytype, with the c-axis normal to the surface (vicinal angle 4°). The epitaxial layer side of the wafer demonstrates a much stronger ASNOM response than the substrate side. To prepare the samples for an experiment (see Fig. 1), the wafer was cut into slices of about $500\mu\text{m}$ in width, and the pairs of such slices were glued onto a metal carrier piece, with their cut surfaces facing up. After the epoxy got hardened, the sample was mechanically polished in order to provide mechanical and optical access to the media. Such a geometry prevents the edges of the wafer from cracking during the polishing procedure, and also allows an easy a comparison between the substrate and the epitaxial-layer edge response. In addition, such a geometry prevents an ASNOM tip from being broken by a sample edge.

A home-built system was used for ASNOM mapping of the sample. A $C^{13}O_2^{16}$ laser was used as a light source to illuminate the tip and to detect the scattered optical signal in a Michelson interferometer scheme by optical homodyning.^{13,14} The light (of amplitude $E_{sc}(\vec{r}_{tip})$ corresponding to the tip location \vec{r}_{tip} with respect to a sample) scattered by an ASNOM tip was collected with an objec-

*To whom correspondence should be addressed

†University of Erlangen

‡Institute for Theoretical and Experimental Physics, Moscow (perm.pos.)

tive and directed back to the photodetector, overlapping the reference beam spot. Since near-field optical interaction between the tip and the surface depends on the tip-sample distance in a non-linear way, the higher harmonic components of a tip oscillation frequency Ω were recovered^{3,15} in the photocurrent oscillations $I_{det}(t)$ as an ASNOm signal $I_{det}^{(n\Omega)}$. Averaging over the reference beam phase was performed in order to exclude arbitrary origin of the reference arm length. With this signal processing, an amplitude of near-field-caused variations in E_{sc} can be acquired (as a complex number):

$$E_{sc}(\vec{r}_{tip}) \propto I_{det}^{(n\Omega)} \propto E_{loc}(\vec{r}_{tip}) \alpha_{eff}^{(n\Omega)}(\epsilon_s(\vec{r}_{tip}), z_0) \quad (1)$$

where $\alpha_{eff}^{(n\Omega)}(\epsilon_s, z_0)$ is an effective tip polarizability,⁹ depending on the surface local dielectric constant $\epsilon_s(\vec{r}_{tip})$ at the tip location. It also depends on the tip vibration amplitude z_0 and its dielectric constant.

Results and discussion

The amplitude and phase maps of an ASNOm signal (oscillations in the photocurrent recovered at the second harmonic of the tip oscillation frequency, and then averaged over full turn of the the reference phase) are shown in the Fig. 2.

Similar to results reported in,⁶ ASNOm image taken at 884cm^{-1} contains no step at all (and simultaneously a SPP wave running from the sample edge is well seen, observed due to a large lateral decay length), then (see image taken at 900cm^{-1}) the SPP wave gets weaker (but still no boundary is visible) and finally a well-pronounced step appears at the frequency of 923cm^{-1} , between the substrate and the epitaxial layers.

Such steps can be well explained by the changes of $\alpha_{eff}^{(n\Omega)}(\epsilon_s(\vec{r}_{tip}), z_0)$ term in (??) caused by \vec{r}_{tip} variations during the sample scanning. A frequency-dependent dielectric function of SiC is commonly¹⁶⁻¹⁹ expressed as the sum of the Lorentzian term (for the lattice) and the Drude

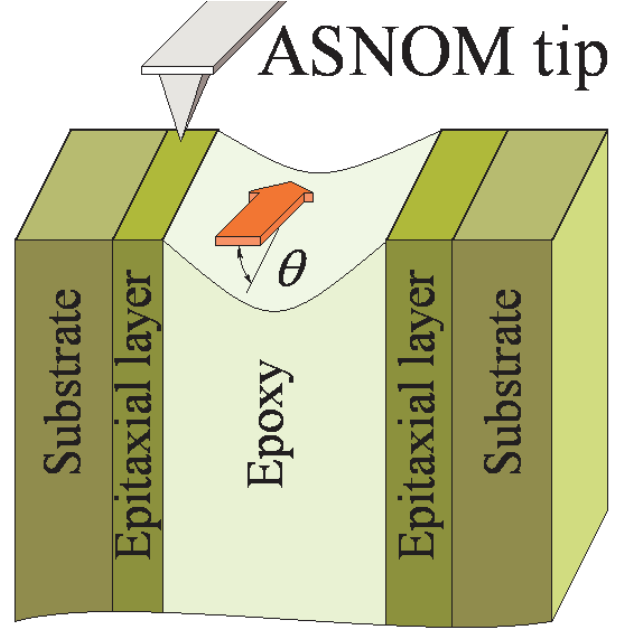


Figure 1: Geometry of the experiment. The slices of a SiC wafer with epitaxial layer were glued together and then polished in order to get mechanical and optical access to the cleaved edge. To make a comparison of ASNOm response on two sides easier, the direction of irradiating light (shown with an arrow) was chosen along the slit between the wafer slices. The direction of the irradiating beam is declined in respect to the surface plane $\theta = 35^\circ$.

term (for the free carrier subsystem):

$$\varepsilon(\omega) = \varepsilon_\infty \left(1 + \frac{\omega_L^2 + \omega_T^2}{\omega_T^2 - \omega^2 - i\omega\Gamma} \right) + \frac{\omega_p^2}{-\omega^2 - i\omega\gamma} \quad (2)$$

The values ω_L and ω_T denote experimentally observed bulk phonon polariton frequencies, Γ is the phonon damping constant. Factor γ in the Drude term denotes the electron subsystem damping constant, and ω_p^2 is the plasma frequency

$$\omega_p^2 = \frac{4\pi N e^2}{m^* m_e} \quad (3)$$

depending on the free carrier concentration N and the effective mass m^* . Strictly speaking, lattice and electron properties of SiC are anisotropic, but for the 4H polytype this difference is just a few percent,²⁰ so it can be neglected in the first approximation. In our calculations, we used the following values:^{21,22} $\omega_T = 797\text{cm}^{-1}$,¹⁸ $\omega_L = 969\text{cm}^{-1}$,¹⁸ $\Gamma = 6\text{cm}^{-1}$,¹⁷ $\varepsilon_\infty = 6.7$. With an electron mass $m_e = 0.4$ we estimate free carrier plasma frequency ω_p as 90cm^{-1} for the epitaxial layer and 8000cm^{-1} for the substrate. Using these values, $\alpha_{eff}^{(n\Omega)}(\varepsilon_s, z_0)$ was calculated. Its dependency on the local dielectric constant of the surface, considered in long-wave dipole approximation⁹ of the Pt-coated²³ tip response in the vicinity of the sample already gives a good fit.

In our case, however, the images acquired with an AS-NOM at the higher light frequency of (see 935cm^{-1} image in Fig. 2) can not be interpreted as just changes in the local value of the sample dielectric function (see term $\alpha_{eff}^{(n\Omega)}(\varepsilon_s, z_0)$ in the (??) expression). Unlike the images presented in⁶ we observe clear wave phenomena, most likely due to less lateral decay of the SPP wave in our samples. A sinusoid-like distribution of $I_{det}^{(2\Omega)}$ amplitude and phase across the epitaxial layer outcrop is clearly seen. It can not be reasonably explained by any distribution of the sample dielectric properties caused e.g. by the doping profile. In this case, additionally to the calculation of a tip effective polarizability in (??) we have to take into account a collective electromagnetic effect, namely an excitation of the running SPP waves by the laser light over all points of the sample surface. A focal spot

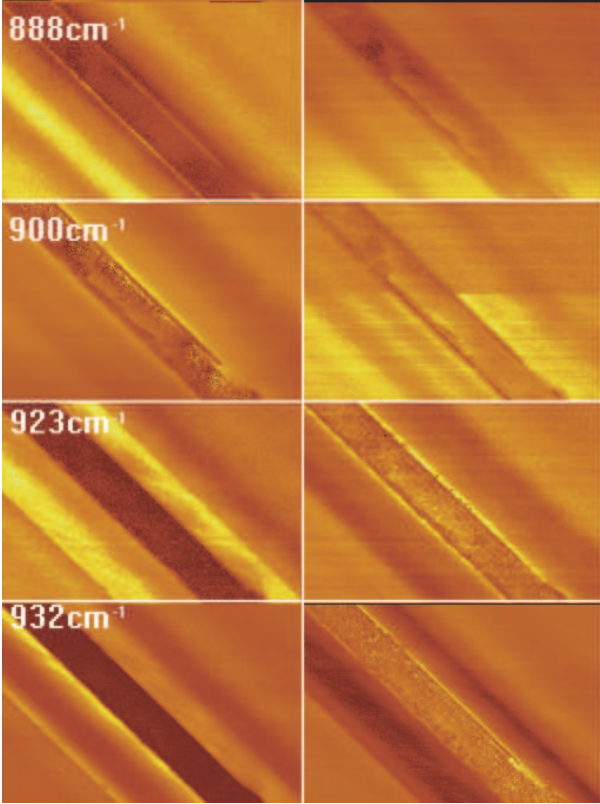


Figure 2: AS-NOM maps of two SiC wafers, prepared in a cleaved-edge geometry. The images were acquired at different light frequencies from 888cm^{-1} to 935cm^{-1} . Left maps represent AS-NOM amplitude $I_{det}^{(2\Omega)}$ collected at 2^{nd} harmonic of the tip oscillation frequency Ω , right ones contain the phase of $I_{det}^{(2\Omega)}$.

of the objective is relatively large ($30 - 50\mu\text{m}$) so that the laser also irradiates some sample area around the tip. The elementary electromagnetic excitations created by a laser light in some other points of the surface, are then delivered as SPP waves to the point of probing. Therefore, we cannot consider a local field amplitude $E_{loc}(\vec{r}_{tip})$ in expression (??) as a constant,²⁴ but have to write it as $E_{loc}(\vec{r}_{tip}) = E_{las} + E_{spp}(\vec{r}_{tip})$ instead. Depending on the phase difference, the interference between these two terms in the sum might be either constructive or (as takes place in Fig.2) destructive.

The homogeneous problem to describe an SPP wave on infinite surface of a polar crystal was solved²⁵⁻²⁷ by substitution

$$E_{spp}(\vec{r}_{xyz}, t) = E_{spp0} e^{i\vec{k}_{xy}(\omega)\vec{r}_{xy}} e^{-\delta_{z(b,a)}z} e^{i\omega t} \quad (4)$$

The problem eigenvalues were found for the lateral propagation term

$$k_{xy}(\omega) = \frac{\omega}{c} \sqrt{\frac{\epsilon_{vac}\epsilon_{SiC}(\omega)}{\epsilon_{vac} + \epsilon_{SiC}(\omega)}}, \quad \epsilon_{vac} \equiv 1, \quad (5)$$

and for the factor $\delta_{z(b,a)}$ describing exponential amplitude decay beneath and above the surface, respectively. To our knowledge, the *inhomogeneous* task of describing SPP wave excitation by an external wave is not solved rigorously yet, in the general case of an arbitrary surface shape.

A dispersion law of the SPP waves calculated with the expressions mentioned above is shown in fig. 3. One can see that the plot curves of different doping level are very close to each other at the frequencies of $880 - 900\text{cm}^{-1}$. At the frequencies of $920 - 940\text{cm}^{-1}$ the curves diverge dramatically. A substrate ($n_N = 7 \cdot 10^{18}\text{cm}^{-3}$) demonstrates more *plasmon*-polariton than *phonon*-polariton behavior, so that the Z-loop on the curve vanishes completely. Therefore, on a cleaved sample side, a strip of undoped epi-layer outcrop appears to be surrounded by the surface media of metal-like electromagnetic properties, with a sharp step at the interface. In such a case, the SPP wave excited on a SiC surface by the irradiating laser light gets confined in a two-dimensional waveguide. As it can

be seen in the Fig. 3, the SPP wavelength at the frequency of 935cm^{-1} gets significantly shorter than at the frequency of 923cm^{-1} . Consequently, a transversal mode field distribution appears in the ASNOm map at 935cm^{-1} , similar to those known for the cm-band waveguides.

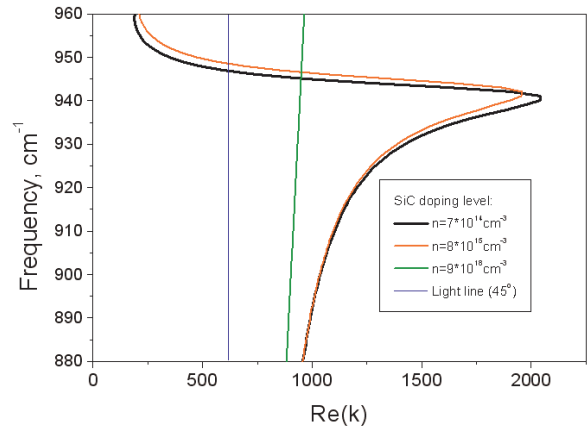


Figure 3: Surface phonon polariton dispersion law plotted for different values of the free carrier concentration in SiC. Most differences occur at the frequencies close to the LO side of the RSB, where the denominator $\epsilon(\omega) + \epsilon_{vac}(\equiv 1)$ in Eq.?? crosses zero.

In conclusion, we studied ASNOm mapping of a doping profile in a 4H-SiC sample. Due to the differences in SiC dielectric function caused mainly by the free carrier plasma in the substrate, we observe clear doping contrast with a lateral resolution of 20nm. The sharp step in the SPP dispersion law on the surface areas of different doping leads, at some light frequencies, to a confinement of the running SPP wave in the strip defined by the outcrop of a low-doped epitaxial layer, similarly to the light confinement in conventional optical fiber.

Acknowledgement

Surface maps were acquired and stored with a help of R9 controller (RHK Tech. MA). The help of K.Kollin (native English speaker) is acknowledged for his kind proof of the text. The work was supported by the German National Science Foundation (DFG grant KA3105/1-1).

Notes and References

- (1) Zenhausern, F.; O'Boyle, M. P.; Wickramasinghe, H. K. *Applied Physics Letters* **1994**, *65*, 1623–1625.
- (2) Zenhausern, F.; Martin, Y.; Wickramasinghe, H. K. *Science* **1995**, *269*, 1083–1085.
- (3) Knoll, B.; Keilmann, F. *Optics Communications* **2000**, *182*, 321 – 328.
- (4) Knoll, B.; Keilmann, F. *Applied Physics Letters* **2000**, *77*, 3980–3982.
- (5) Huber, A. J.; Keilmann, F.; Wittborn, J.; Aizpurua, J.; Hillenbrand, R. *Nano Letters* **2008**, *8*, 3766–3770, PMID: 18837565.
- (6) Huber, A.; Ocelic, N.; Taubner, T.; Hillenbrand, R. *Nano Letters* **2006**, *6*, 774–778, PMID: 16608282.
- (7) Knoll, B.; Keilmann, F. *Nature* **1999**, *399*, 134–137.
- (8) Taubner, T.; Hillenbrand, R.; Keilmann, F. *Applied Physics Letters* **2004**, *85*, 5064–5066.
- (9) Hillenbrand, R.; Knoll, B.; Keilmann, F. *Journal of Microscopy* **2001**, *202*, 77–83.
- (10) Hillenbrand, R.; Keilmann, F. *Applied Physics Letters* **2002**, *80*, 25–27.
- (11) Huber, A.; Kazantsev, D.; Keilmann, F.; Wittborn, J.; Hillenbrand, R. *Advanced Materials* **2007**, *19*, 2209–2212.
- (12) Stiegler, J. M.; Huber, A. J.; Diederhofen, S. L.; Gómez Rivas, J.; Algra, R. E.; Bakkers, E. P. A. M.; Hillenbrand, R. *Nano Letters* **2010**, *10*, 1387–1392, PMID: 20302289.
- (13) Keilmann, F.; Hillenbrand, R. *Philosophical Transactions: Mathematical, Physical and Engineering Sciences* **2004**, *362*, 787–805.
- (14) Taubner, T.; Keilmann, F.; Hillenbrand, R. *Nano Letters* **2004**, *4*, 1669–1672.
- (15) Wurtz, G.; Bachelot, R.; Royer, P. *Review of Scientific Instruments* **1998**, *69*, 1735–1743.
- (16) Tiwald, T. E.; Woollam, J. A.; Zollner, S.; Christiansen, J.; Gregory, R. B.; Wetteroth, T.; Wilson, S. R.; Powell, A. R. *Phys. Rev. B* **1999**, *60*, 11464–11474.
- (17) Harima, H.; ichi Nakashima, S.; Uemura, T. *Journal of Applied Physics* **1995**, *78*, 1996–2005.
- (18) Sasaki, Y.; Nishina, Y.; Sato, M.; Okamura, K. *Phys. Rev. B* **1989**, *40*, 1762–1772.
- (19) Yugami, H.; Nakashima, S.; Mitsuishi, A.; Uemoto, A.; Shigeta, M.; Furukawa, K.; Suzuki, A.; Nakajima, S. *Journal of Applied Physics* **1987**, *61*, 354–358.
- (20) Adolph, B.; Tenelsen, K.; Gavrilenko, V. I.; Bechstedt, F. *Phys. Rev. B* **1997**, *55*, 1422–1429.
- (21) Bimberg, D.; Blachnik, R.; Cardona, M.; Dean, P.; Grave, T.; Harbeke, G.; Hübner, K.; Kaufmann, U.; Kress, W.; Madelung, O.; Münch, W. v.; Rössler, U.; Schneider, J.; Schulz, M.; Skolnick, M. In *Physics of Group IV Elements and III-V Compounds*; Hellwege, K.-H., Madelung, O., Eds.; Springer, Berlin, 1982.
- (22) Bechstedt, F.; Kaeckell, P.; Zywietz, A.; Karch, K.; Adolph, B.; Tenelsen, K.; Furthmueller, J. *physica status solidi (b)* **1997**, *202*, 35–62.
- (23) Ordal, M. A.; Bell, R. J.; R. W. Alexander, J.; Long, L. L.; Querry, M. R. *Appl. Opt.* **1985**, *24*, 4493–4499.
- (24) In our setup, the tip is always located in the focus of the objective, so that the amplitude and especially phase of the laser light at the tip location are constant.

- (25) Lyddane, R. H.; Sachs, R. G.; Teller, E. *Phys. Rev.* **1941**, *59*, 673–676.
- (26) M. Born, K. *Dynamical Theory of Crystal Lattices*; Oxford University Press, New York, 1954.
- (27) Barron, T. H. K. *Phys. Rev.* **1961**, *123*, 1995–1998.